CERN/ISRC/70-5

17.4.1970

PROPOSAL FOR A TEST AND SURVEY EXPERIMENT AT THE ISR.

G. Charpak, D. Drijard, J. Favier, G. Fischer,

B. Hyams, A. Minten and F. Sauli - (CERN);

G. Flügge (Hamburg);

M. Bott-Bodenhausen (München);

G. Coignet (Orsay);

N. N. (Princeton);

Ch. Gottfried (Wien).

PS/160

1. INTRODUCTION

In 1971 the CERN Intersecting Storage Rings will start operating, and in 1972 a large experimental magnet[1] will be installed at the intersect 4. The above group, formed of CERN staff and visitors at CERN, will provide the necessary experimental equipment, as far as it is standard and can be used for several experiments. This equipment includes a set of large multi-wire proportional chambers[2] with the corresponding electronics, on-line computers and a basic analysis program chain.

The final configuration will be available for experiments at the end of 1972. We suggest, however, that parts of the apparatus should operate at an earlier date and then gradually build up to the final complete system. Furthermore, the physicists involved in the construction intend to gain experience during the first phase of ISR operation.

We therefore propose a test and survey experiment which serves a triple purpose:

i) to test the proportional chambers, the special electronics connected to them, the on-line operation with the computers, and a preliminary analysis chain;

ii) to gain experience in the specific environment at the ISR, investigating background, trigger conditions for beam-beam interactions, and luminosity and calibration questions;

iii) to perform some simple survey measurements on relatively abundant processes, such as multiparticle production (section 3), and a search for diffraction

reactions (section 4).

This proposal updates and completes the program given already to the ISRC in October 1969[3].

2. DETECTION SYSTEM

The detector to be operated in the SFM has to fulfill several conditions: It should

- be insensitive to magnetic field;
- have high spatial resolution in order to make best use of the field;
- be flexible enough to be adapted to different experiments;
- be movable to be adapted to the magnet on-off condition, and to allow baking of the vacuum chambers;
- be reliable to be operated in an inaccessible experimental area.

To satisfy the above criteria we have chosen a detector consisting essentially of multiwire proportional chambers[2]. A prototype of a first standard chamber has been constructed, based on the experience gained so far in our and other groups[4) 5)], and is being tested now.

2.1. Proportional Chambers

The geometrical configuration of the prototype is shown in Fig. 1. Nonmagnetic materials, such as Vetronite, and aluminum, have been used to construct modular frame units of 7mm thickness and outside dimensions of 54x185 cm. Electrodes, i.e. either HV or wire planes, are separated by one module. Several modules can be assembled together in order to give a chamber with a desired number of planes. The chamber is mechanically stiffened by an aluminum frame attached on one side of it. The special cut-out on one side of the chamber will allow to extend the sensitive area of the chamber as near as 50mm from the beam axis, assuming an elliptical vacuum pipe of 60mm height. The prototype consists of three independent wire planes, one horizontal, and two at $\pm$ 60°. The wire distance

is 2mm, and the prototype has about 1200 wires. One preamplifier per wire is attached on the chamber frame, and twisted-pair ribbon cables then transport the signal to the control-room outside the experimental area. This separation is useful since it reduces the electronics volume in the magnet gap and brings the major part of the electronics to an accessible environment.

2.2. Electronics

The diagram of the wire electronics is shown in Fig. 2a. The wire is connected to a differential preamplifier PA, after which the signal is transferred over ~ 30m through flat, 32 twisted-pair cables to the control-room. There the pulse is processed by a receiver and shaper R, a delay D, a memory gate MG and a memory M. The delay, achieved by a monostable with a mean pulse length of 250 nsec., allows for logical decision to be taken before accepting the event in the memory. By changing a reference voltage, it is possible to cover the delay range between 200 and 300 nsec for the whole system. The decision logics incorporates the self-triggering facility of the chambers; it is initiated by the front edge of the delay pulse, and timing or logical decisions can be based on signals from groups of 32 wires. The instant logics (Fig. 2b) permits these decisions to be taken within the intrinsic time resolution of the proportional chambers, less then 50 nsec in our case.

After this special circuitry a second slow level of decision (DC logics) is followed by a readout device, leading to the on-line computer (EMR 6130, 16 bit, 0.780 µsec). This small computer will be later linked to a CII 10070 (Omega main computer). The computer will read the proportional chambers, and it will control the run (on-off-reset) and check parameters such as gas pressures

and high voltages. Finally it will control an automatic test facility for the chambers. We imagine a test procedure which:

(i) searches discharges or oscillations by looking for fixed bits appearing in consecutive random triggers;

(ii) searches for empty bits when exposing all wires of one chamber to a small pulse on the HV mesh synchronized with a strobe on all memory gates of this chamber.

2.3. Performance

Our standard chambers will have a 7.2mm gap between HV and wire plane, a 2mm wire distance and an A-CO_2 gas filling. For these conditions an intrinsic time jitter of 30 nsec has been measured[4]. Allowing for an additional jitter from electronics, a 60 nsec strobe will ensure full efficiency. These 60 nsec will be the time resolution of the system. The dead time on each wire is determined by the delay D and should be about 4 times the delay time, i.e. $\sim$1 µsec. Note that for 10^6 ten-prongs/sec, equally distributed over a 1000 wire plane the loss due to dead time is 1%o. The spatial accuracy for 2mm wire distance has been experimentally measured, and results in a standard deviation of $\pm$ 0.57mm.

3. SURVEY ON MULTIPARTICLE PRODUCTION (1971)

The first period of ISR operation (2nd half of 1971) is largely determined by safe running-in conditions for the accelerator. For the experiments this means that only vacuum chambers with rather thick walls and no special windows or flares will be available. Hereby the

measurement of forward particles is greatly disturbed. We therefore will concentrate during this time on the detection of large angle particles.

3.1. Physics

Lacking of any complete theory for "inelastic" processes, multiparticle production has been described in a number of approaches, such as the

- thermodynamical theory[6];
- the two-fireball model[7];
- the isobar pionization model[8];

These different descriptions can be tested by the measurement of overall properties, as there are

- production spectra of π, K, N etc., as function of momentum and angle;
- average multiplicity and multiplicity distribution;
- correlations between particles produced.

Since no means of particle identification and momentum measurement will be available in our case, we will concentrate on the second of the above points.

We will measure:

i) the average multiplicity of secondary particles produced by the collision of two protons colliding at E_{CM} = 50 GeV;

ii) the multiplicity distribution of the secondaries;

iii) the angular distribution of the secondaries; (note, that the particle angles are measured

in the laboratory system, which moves with $\beta_{CM} \approx 0.13$ perpendicular to the intercept of the colliding beams with respect to the CM. Without knowledge of momenta the exact re-transformation is not possible, but, in view of the small value of β_{CM}, a correction should be possible with assumptions on the momentum distribution and on the isotropy of the angular distribution around the line of collision in the CM).

Essential byproducts will be the determination of the shape of the interaction diamond by reconstruction of the vertices and a measurement of the beam overlap distribution

$$\int \rho_1(z)\rho_2(z)dz \propto h_{eff}^{-1}$$

3.2. Experiment

The measurements described above require a detector arrangement of almost 4π acceptance. On the other hand, we will have to meet a number of restrictions due to the initial phase of operation of both the ISR and the detection system:

- a very simple, thick walled vacuum chamber limits particle detection, due to interactions and multiple scattering, to angles $\gtrsim$ 200 mrad;
- only a detector of limited size, probably $< 10^4$ wires of proportional chambers, will be available at that time.

We intend to start with a simple arrangement of 7 proportional chambers of the standard size (Fig. 3a). Each chamber contains three wire planes. Double chambers on three sides allow vertex

reconstruction and measurements of the beam overlap distributions in both the vertical and horizontal planes. The precision of reconstruction should be of the order of $\pm$ 1mm for particles emerging at large angles with respect to the vacuum chamber.

In view of the maximum acceptance it is desirable to place 4 additional chambers in the forward-backward direction (Fig. 3b). With these chambers, however, one will encounter some background problems due to beam-gas interactions of the incoming beams, which have to be studied in more detail.

3.3. Acceptance Calculations

In order to obtain an estimate of the angular and multiplicity acceptances we performed a Monte Carlo-calculation, generating events with a mean multiplicity of about 12 and a reasonably flat multiplicity distribution (Fig. 4a).

The angular and momentum distributions of the secondaries were chosen to follow the predictions of the thermodynamical model[9], which, at the same time, yields the known $p_\perp \exp(-p_\perp/0.2)$ distribution of transverse momentum.

It should be noted that the θ-distribution (see Fig. 4b) is rather sharply peaked at small angles. Therefore we find an overall particle acceptance of only 39% for the experimental setup of Fig. 3a, whereas we see 63% of all particles with the additional chambers of Fig. 3b. All results quoted below have been obtained with the complete arrangement (Fig. 3a and b).

According to the limited acceptance, the "measured" mean multiplicity decreases to 7.8. Correcting for the percentage of lost particles one can get back the right mean value and multiplicity

distribution (Fig. 4a). Generally, however, this procedure is quite model-dependent and in the actual experiment one has to take account of the correlations between the angular distributions and the multiplicity.

The results shown in Fig. 4b indicate that we can obtain angular distributions for $\theta_{lab} \geq 200$ mr with reasonable accuracy. The kinematical transformation back to the center-of-mass system (already quoted above) does not seriously affect the θ-distribution. On the other hand, the distribution of the azimuthal angle ϕ, which is isotropic in the CM-system, gets quite asymmetric in the lab (see Fig. 4c). In this case one can test suitable momentum distributions to get back isotropy in the CM-system.
The conversion of γ-rays in the vacuum chamber would be determined seperately to correct the measured charged multiplicity.

4. SURVEY OF DIFFRACTION REACTIONS (1972)

In this phase of ISR operation the use of special vacuum chambers is expected to be possible so that the measurement of small angle particles becomes feasible. We propose to perform during this phase an initial search for and a study of diffraction processes.

4.1. Physics

It is expected that those two-body or quasi-two-body final states which can be produced by diffraction (or Pomeron exchange) will dominate at high energies. The processes belonging to this class are:

(1) $pp \rightarrow pp$

(2) $pp \rightarrow p\overset{x}{\underset{\hookrightarrow \pi^+ n}{N}}$

(2') $pp \rightarrow p\overset{x}{\underset{\hookrightarrow p\pi^+\pi^-}{N}}$

(3) $pp \rightarrow \overset{x}{\underset{\hookrightarrow \pi^+ n}{N}} \quad \overset{x}{\underset{\hookrightarrow \pi^+ n}{N}}$

The N^x refers to the family of isobars with isospin $\frac{1}{2}$ and parity $(-1)^{\Delta J}$ where ΔJ is the isobar spin minus $\frac{1}{2}$ [10].

There is some knowledge on the behaviour of reaction (1) at higher energies[11]. Reaction (2) was studied up to 29 GeV[12], reaction (3) has not been investigated at present accelerator energies.

It was discussed earlier[13], [14] that the reconstruction of the above reactions is possible in a 2C, 1C, 0C, 0C fit, respectively, if the directions of all secondaries are measured. The elastic reaction is used as a monitor. Cross sections and rate estimates are given in table 1. Simultaneously the cross section (or, at least, an upper limit of it) for the exchange process

(4) $pp \rightarrow n\,\overset{x^{++}}{\underset{\hookrightarrow p\pi^+}{N}}$

can be obtained.

4.2. Detector

The detector is shown schematically in Fig. 5. It is built up of SFM standard chambers (For neutron detector see also appendix). Anticounters (not shown) cover the solid angle not subtended by the detector.

4.3. Acceptance and Resolution

Acceptance calculations have been done for the reactions 1, 2 and 3 with the following conditions:

- a vacuum chamber, symmetrical in both directions, with a flare of 50cm radius at a distance of 5 meters from the intersect, and an elliptical tube continuing from there on;
- standard chambers perpendicular to the beam at distances of 5.1 meters and 7.35 meters. The chambers were assumed to be sensitive at 5cm distance from the beam axis;
- neutron chambers with the same geometry at a distance of 7.5 meters from the intersect.

The results of the Monte Carlo calculations for reactions (1) to (3) are given in Fig. 6 and 7, respectively. An isobar mass of 1470 MeV was used, and a variation of the differential cross section with e^{10t} was assumed.

The resolution of the reconstruction was tested by

- generating events in a M.C. procedure;
- digitizing them with a precision of $\pm$ 1mm for charged particles and $\pm$ 8mm for neutrons;
- processing the digitizations by the SFM pattern recognition and reconstruction programs[15].

The result is shown in Fig. 8a by the effective mass distribution for a zero width isobar with a mass of 1470 MeV.

4.4. Background

Extensive background calculations have been done for reactions (1) and (2) only. The background for reaction (1) consists of inelastic

events which produce two accidentally collinear (in the CM) charged particles and no other charged particles traversing the chambers (the existence of the anticounters was ignored in this consideration). These are:

$$pp \rightarrow (\text{everything}) + \pi^+\pi^+\pi^-\pi^-$$
$$pp \rightarrow pN^x \rightarrow pp\,(\pi^o)$$
$$pp \rightarrow N^xN^x \rightarrow \pi^+(n)\pi^+(n)$$
$$pp \rightarrow N^xN^x \rightarrow p\,(\pi^-)\,p\,(\pi^o)$$

The following production ratios were used:
all inelastic: $pp : pN^x : N^xN^x = 3 : 1 : 0.1 : 0.01$

The first reaction was generated according to a CKP formula[16], the others in the standard way using a t-dependence of e^{10t}, as it was also used for the elastic reaction. Fig. 6 shows the t distribution for events defined as collinear by a cut at $\pm$ 2 mrad. The figure does not indicate any background problem up to $t \simeq -0.5\ (\text{GeV}/c^2)^2$.

The background of reaction (2) was investigated for the following processes

i) $pp \rightarrow p + N^x \rightarrow p + n\,\pi^+(\pi^o)$
ii) $pp \rightarrow N^x+N^x \rightarrow (n)\pi^+ + n\pi^+$
iii) $pp \rightarrow N^x+N^x \rightarrow p(\pi^o) + n\pi^+$

The background events were simulated and then processed like genuine events. The number of the accepted background events and of those having passed the fit are displayed in table 2. Fig. 8a shows the (πn)- invariant mass distribution of the successfully fitted events from reaction i). Fig. 8b shows the t-distribution of these events. The contribution of reactions ii) and iii) to the distributions of Fig. 8a and 8b were deliberately omitted since

their (πn)-invariant mass distributions are flat over a wide energy range, their production cross section is small and the rejection rate of the fit very high.

The experimental result will be the sum of the histograms in Fig.8a (widened by the intrinsic width of the N^{x}), assuming equal yields for both processes. We conclude, that a separation by purely kinematical methods is difficult. Therefore three sets of anticounters, one around the intersect, and two shielding the downstream region not covered by the main detector, will be inserted. The anticounters, consisting of lead-scintillator sandwiches, will be effective for charged particles and γ-rays. Fig. 8b shows the expected background reduction for the background reaction discussed above, assuming a detection efficiency of 95%.

Table 1: $pp \rightarrow pp$

θ [mrad]	t $[GeV^2/c^4]$	$\frac{d\sigma}{dt}$ $[cm^2/GeV^2c^{-4}]$	$\frac{d\sigma}{d\Omega}$ $[cm^2/sterad]$	counts/sec.mrad
0	0.	$80.5 \cdot 10^{-27}$	$16.0 \cdot 10^{-24}$	------
10	0.0625	43.1	8.56	41
15	0.141	19.6	3.90	390
20	0.250	6.6	1.31	250
25	0.391	1.61	0.32	76
30	0.563	0.29	$57.6 \cdot 10^{-27}$	17
40	1.000	$3.62 \cdot 10^{-30}$	0.72	0.3
50	1.563	0.013	$2.59 \cdot 10^{-30}$	0.001

NOTE: 1) The cross section is computed on the basis of

$$\frac{d\sigma}{dt} = \frac{\sigma^2_{tot}}{16\pi} e^{bt} = \frac{\pi}{k^2} \frac{d\sigma}{d\Omega}$$

σ_{tot} = 40 millibarn, b = 10 $\left[GeV/c^2\right]^{-2}$,

k = proton CM momentum;

2) rates were calculated using the acceptance calculations from Fig. 6 and the nominal luminosity of 4.10^{30} $\left[cm^{-2}sec^{-1}\right]$.

Table 2:

Reaction	Generated Events	Accepted Events	Fitted Events
$pp \to pN^x$ $\to pn\pi^+$	45000	778	666
$pp \to pN^x$ $\to pn\pi^+\pi^o$	45000		
i) π^o undetected		991	317
ii) n undetected and γ simulates neutron		392	49
$pp \to N^xN^x$ $\to n\pi^+n\pi^+$ (one n undetected)	45000	1267	64
$pp \to N^xN^x$ $\to p\pi^on\pi^+$ (π^o undetected)	45000	1133	147

(Appendix) CERN/ISRC/70-5

NEUTRON DETECTOR

The detection of the neutron in the N* decay is essential to reconstruct the reaction $pp \rightarrow pn\pi^+$ in an experiment without the magnet, and gives an obvious advantage in mass resolution with the split field magnet[17].

Considering the kinematics of N* production and decay, we are faced with the problem of detecting neutrons in the momentum range 5 - 25 GeV/c, and emitted in the laboratory between 0° and 5° with respect to the N* direction (at first approximation we can consider this direction as that of the I.S.R. circulating proton). We want to measure the neutron direction with an uncertainty of the order of $\pm$ 1 mrad.

Neutrons will be detected by observing the charged particles produced in nuclear reactions. The exact calculation of all the various interaction mechanisms is difficult. To study a possible detector, we have therefore used experimental results instead of trying a long and difficult Monte Carlo calculation[18]. For that purpose, we have scanned about 500 pictures taken by the Karlsruhe group in an elastic n-p scattering experiment[19] performed in a neutron beam having a momentum range of 3 - 20 GeV/c, and a maximum intensity around 9 GeV/c. An optical spark chamber arrangement with thin (1.5 and 3mm) iron plates in between served to detect the scattered neutrons.

The scanning shows several features:

a) The mean multiplicity at the vertex (without counting the slow backwards particles) is 2.8; this number decreases slowly with an increasing amount of iron after the vertex:

cm of iron behind the vertex	mean multiplicity
0	2.8
5	2.6
10	2.2
15	1.6

This fact indicates that we can consider using thick converters, thus decreasing the number of detectors and the price.

b) The mean maximum angle of the secondaries is 32°.

c) In about 37% of the events, we have one or several backwards tracks able to cross about 0.5cm of iron.

d) We have deduced from the density of the events along the detector, a "detectable" collision length $\lambda_D = 15.5$cm, related to the usual collision length λ_{col} by the proportion.

$$\lambda_D = 1.2\ \lambda_{col}$$

So we can use the following efficiency formula:

$$\varepsilon = 1 - \exp(-L/\lambda_D)$$

For example, $\varepsilon \simeq 0.5$ for 10cm of iron.

We first considered a sandwich detector compound of 4cm thick blocks of brass seperated by XY proportional wire chambers, using the barycentres of the jets seen in the chambers to obtain the neutron impact point. As an alternative, we studied the following detector, which for the same price gives a space resolution three times better.

It consists (Fig. 9) of two identical modules, each compound of a $10 \times 150 \times 50 cm^3$ brass converter, followed by two XY proportional wire

chambers at 10 and 30cm distance. These can be of the "standard" type, with 2mm wire spacing, but in clustering 3 or 4 wires to the same amplifier. So we get two points for each outgoing track and we can reconstruct the vertex inside the converter. The accuracy obtained with the events of the film for the coordinate perpendicular to the axis of the detector is.

$$\sigma_x = 0.4\text{cm} \ (\pm\ 0.5 \text{ mrad at } 8 \text{ meters})$$

to compare with $\sigma_x = 1.2$cm in the barycentre method. The efficiency for a two modules' detector will be better than 0.64.

$$\varepsilon \geq 0.64$$

(it is lower than ε given by the formula since some events have no tracks able to cross all the converter, and others are rejected by the vertex program).

Considerations of accuracy (bound to the length of the converter), magnetic field and price have determined our choice for brass as converting material. We choose proportional chambers essentially for their time resolution, needed by the "hot" region where the neutron detector will operate.

A γ detector consisting of a standard lead-scintillator sandwich will be placed in anticoincidence before the neutron detector. In having a loss in neutron efficiency in the range of 15% of ε, we can have a γ efficiency of 0.95 with 2cm of total lead thickness. The 5% of remaining γ can be in part eliminated by selections on the events configuration.

The final efficiency can be 60%. It will have to be measured before the experiment.

REFERENCES:

1. L. Resegotti, ISR-MAG 69-58

2. G. Charpak, R. Bouclier, T. Bressani, J. Favier, C. Zupancic, Nuc. Instr. and Meth., 62 (1968) 262

3. G. Charpak, A. Minten, L. Resegotti, CERN ISRC/69-54.

4. G. Charpak, D. Rahm and H. Steiner
Nucl. Instr. Meth., 80 (1970) 13
R. Bouclier, G. Charpak, G. Coignet, Z. Dimcovski, G. Fischer, G. Flügge and F. Sauli
(to be published)

5. J.H. Dieperink, K. Kleinknecht, P. Steffen and F. Vanucci
NP Int. Report 69-25 (1969)

G. Amato, E. Chesi, P. Declais and J. Séguinot, private communication (March 1970)

6. R. Hagedorn and J. Ranft
Nuovo Cimento Suppl. 6, 169 (1968)

7. G. Cocconi, Ph. Rev. 111, 1699 (1958)
K. Niu, Nuovo Cimento 10, 994 (1958)

8. Y. Pal, B. Peters, Nat. Fys. Medd. Dan. Vid. Selsk, 33, No.15 (1964)

9. S. Anderson and C. Daum, Computer program for calculation of particle production spectra for the ISR (CERN 1969)

References cont'd

10. D.R.O. Morrison, Phys. Rev. 165 (1968), 1699

11. Recent experiments at Serpukhov indicate a further shrinkage of the pp diffraction peak. The extrapolation of this observation to ISR energies results in a value of the parameter $b \approx 15$ $(GeV/c^2)^{-2}$. (A.M. Wetherell, private communication)

12. For reference see: E. Lillethun, in Proceedings of the Lund International Conference on Elementary Particles, Lund 1969, page 167.

13. M. Bott-Bodenhausen, W. Koch, U. Stierlin, B.D. Hyams and G.K. O'Neill, CERN-ISRC/69-8 and /69-8 Add.

14. G.K. O'Neill, CERN/NP/434 (1969)

15. We want to acknowledge the important contribution of Dr. H. Grote to the development of the analysis programs.

16. G. Cocconi, L.J. Koester and D.H. Perkins, UCRL-10022 (1961).

17. Proposal to measure the dependence of isobar excitation in proton-proton collision at I.S.R. CERN-Hamburg-Orsay-Vienna Collaboration (CERN/ISRC/69-14).

18. G. Coignet, J. Favier, NP Int. Rep. (to be distributed).

19. J. Engler, K. Horn, J. König, F. Mönning, P. Schludecker, H. Schopper, P. Sievers, H. Ullrich and K. Runge, Phys. Lett. 29B, 321(1969).

FIGURE CAPTIONS

Fig. 1 SFM standard proportional wire chamber.

Fig. 2 a) Wire electronics
b) Block diagram of the proportional chamber electronics.

Fig. 3 Chamber setup for the initial experimentation at the ISR
a) large angle chambers;
b) small angle chambers.

Fig. 4 a) Multiplicity distributions
upper part: input distribution of Monte Carlo calculation;
lower part: distribution accepted by the apparatus (shaded) and distribution corrected for particle losses;
b) Distributions of the polar angle θ_{lab};
c) Distributions of the azimuthal angle ϕ_{lab}.

Fig. 5 Detector for diffraction reactions.

Fig. 6 t- distribution of accepted genuine and background events for the process pp→pp.

Fig. 7 t- distributions of generated and accepted events of the processes $pp \to pN^X$ and $pp \to N^X N^X$.

Figure Captions cont'd

Fig. 8 Resolution and background rejection for the process $pp \to pN^{x} \to p\pi^{+}n$.

a) resolution curve for a zero width resonance and effective $(n\pi^{+})$ mass distribution for the background decay $N^{x} \to n\pi^{+}\pi^{o}$;

b) t- distribution of genuine and background events.

Fig. 9 Neutron detector consisting of anticounter , two converters and two proportional chambers per converter.

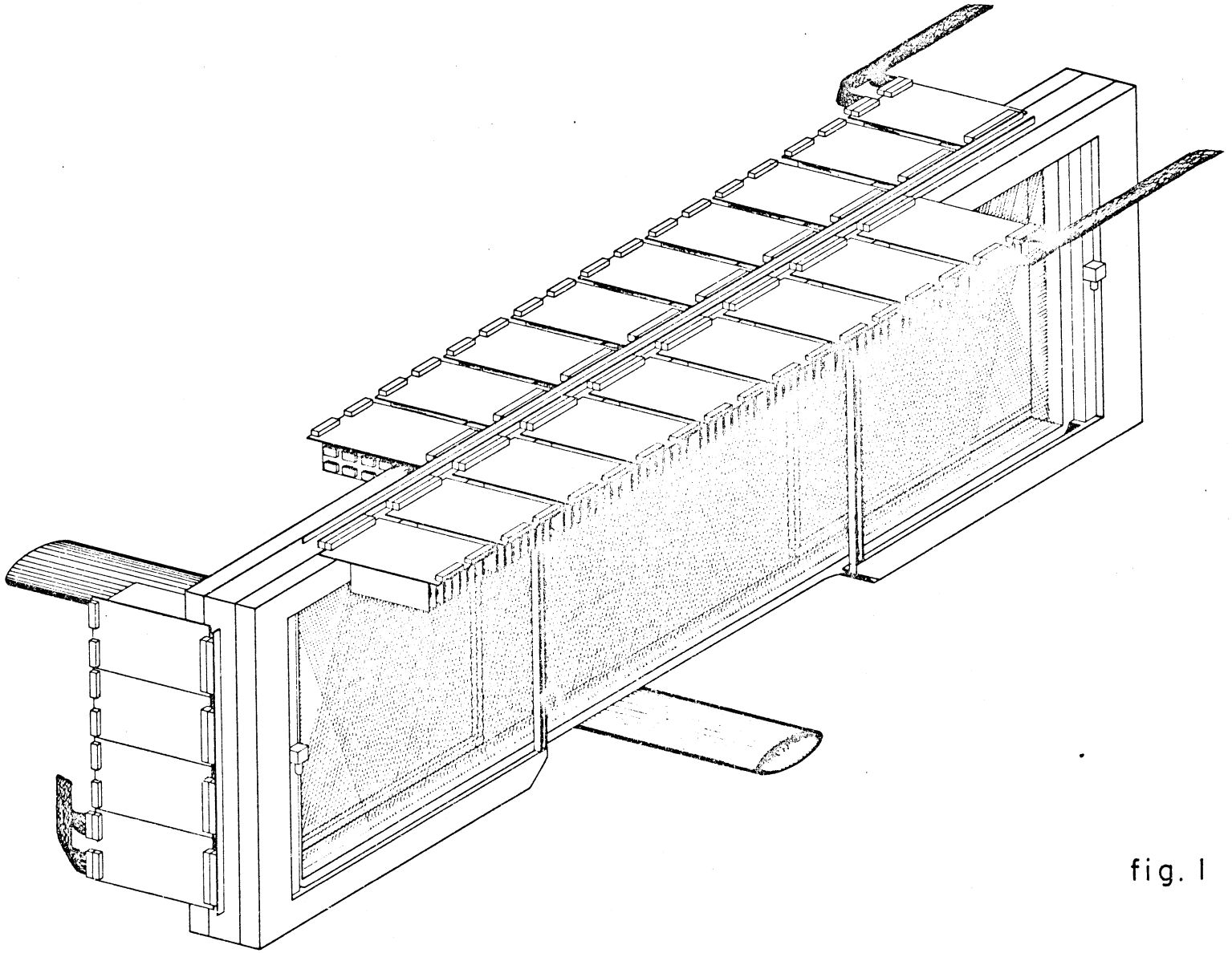

fig. 1

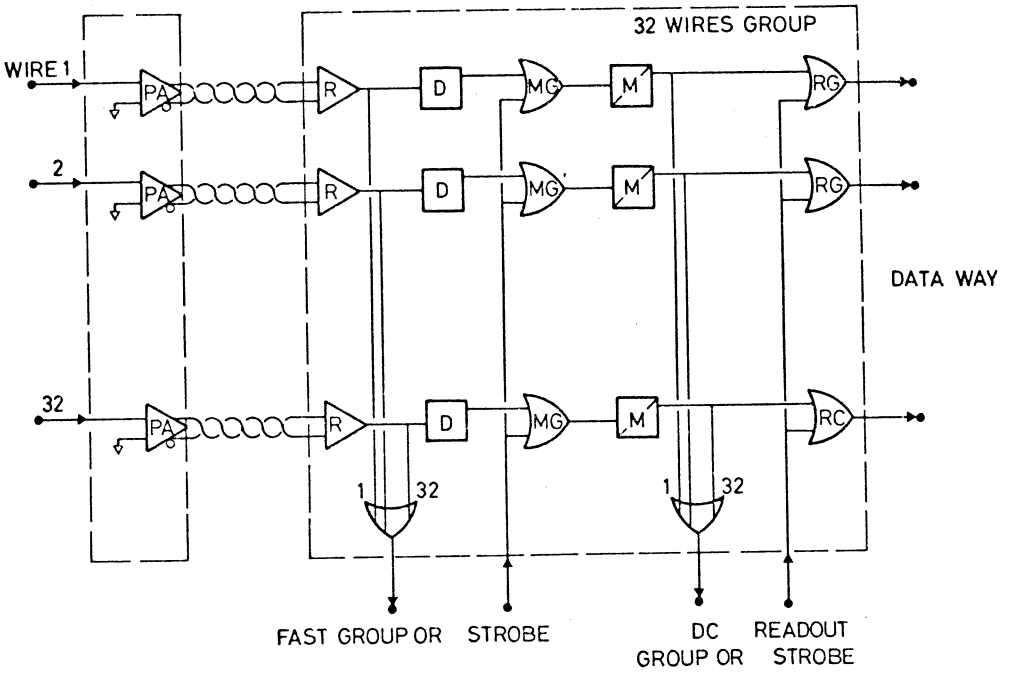

fig. 2a GROUP ELECTRONICS ORGANIZATION

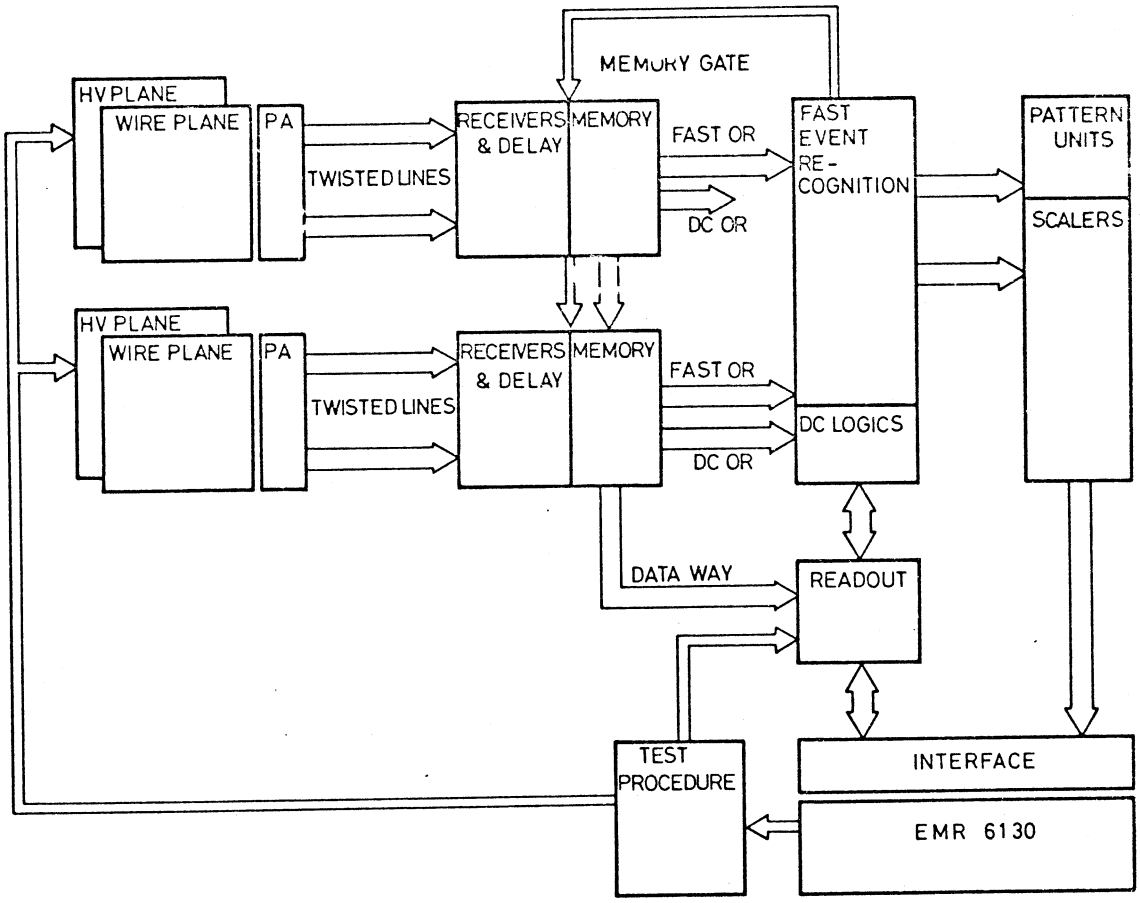

fig. 2b DETECTOR AND READOUT BLOCK DIAGRAM

FIG 3a

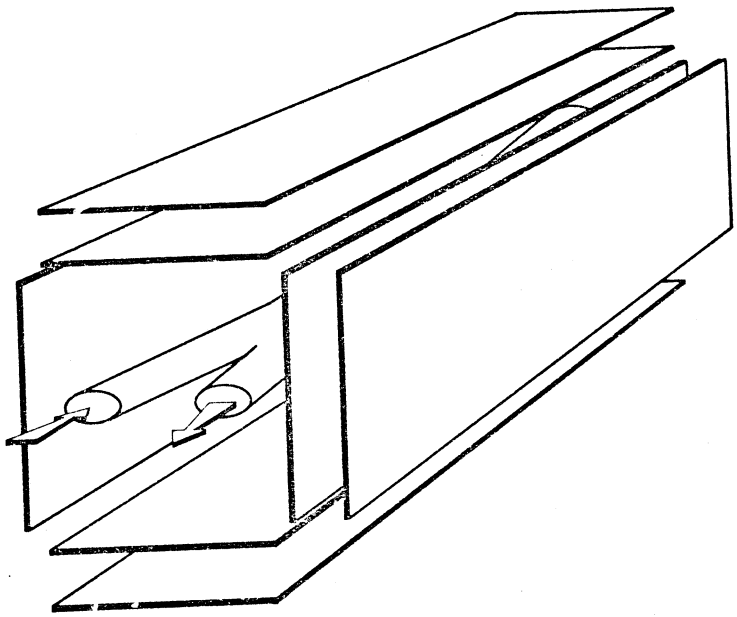

FIG 3b

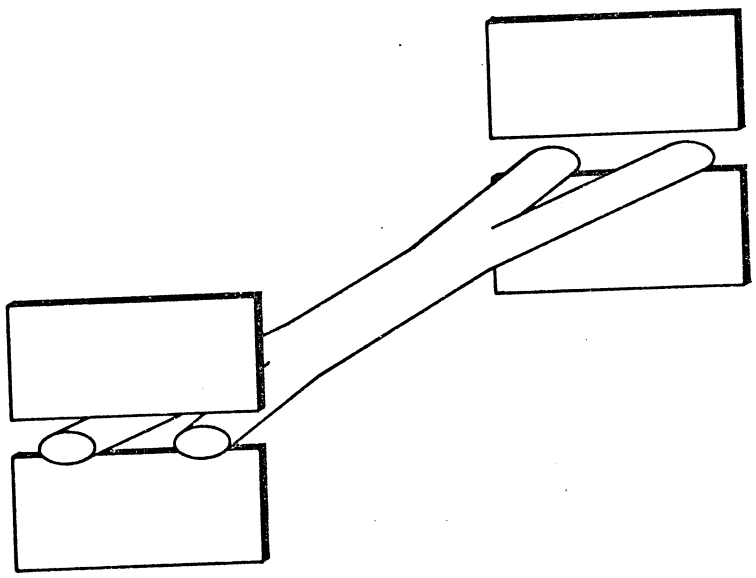

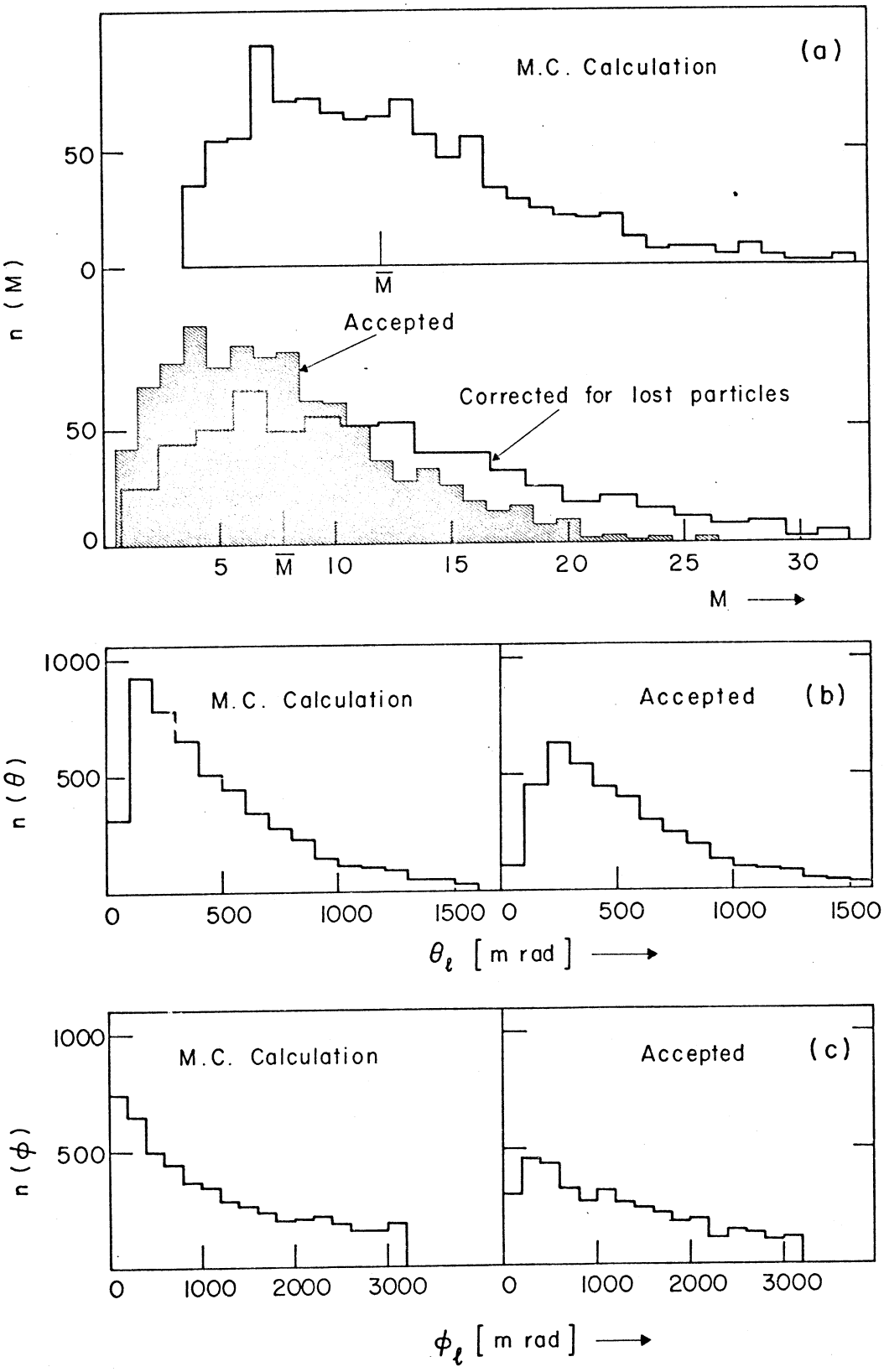
(a)
M.C. Calculation
n (M)
50
0
$\bar{M}$
Accepted
Corrected for lost particles
50
0
5
$\bar{M}$
10
15
20
25
30
M
(b)
M.C. Calculation
Accepted
n (θ)
1000
500
0
500
1000
1500
θ_ℓ [m rad]
(c)
M.C. Calculation
Accepted
n (φ)
1000
500
0
1000
2000
3000
ϕ_ℓ [m rad]

fig. 4

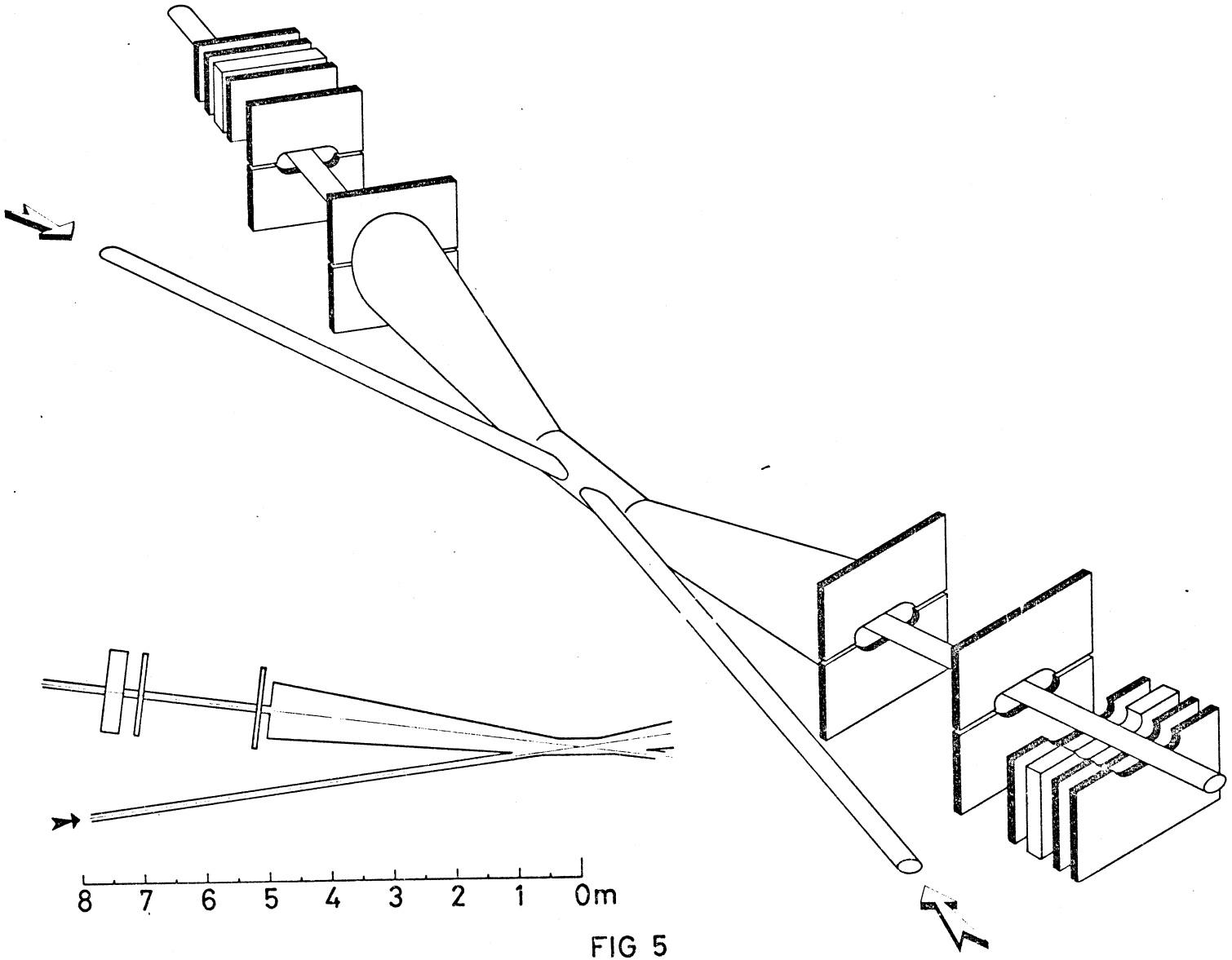

FIG 5

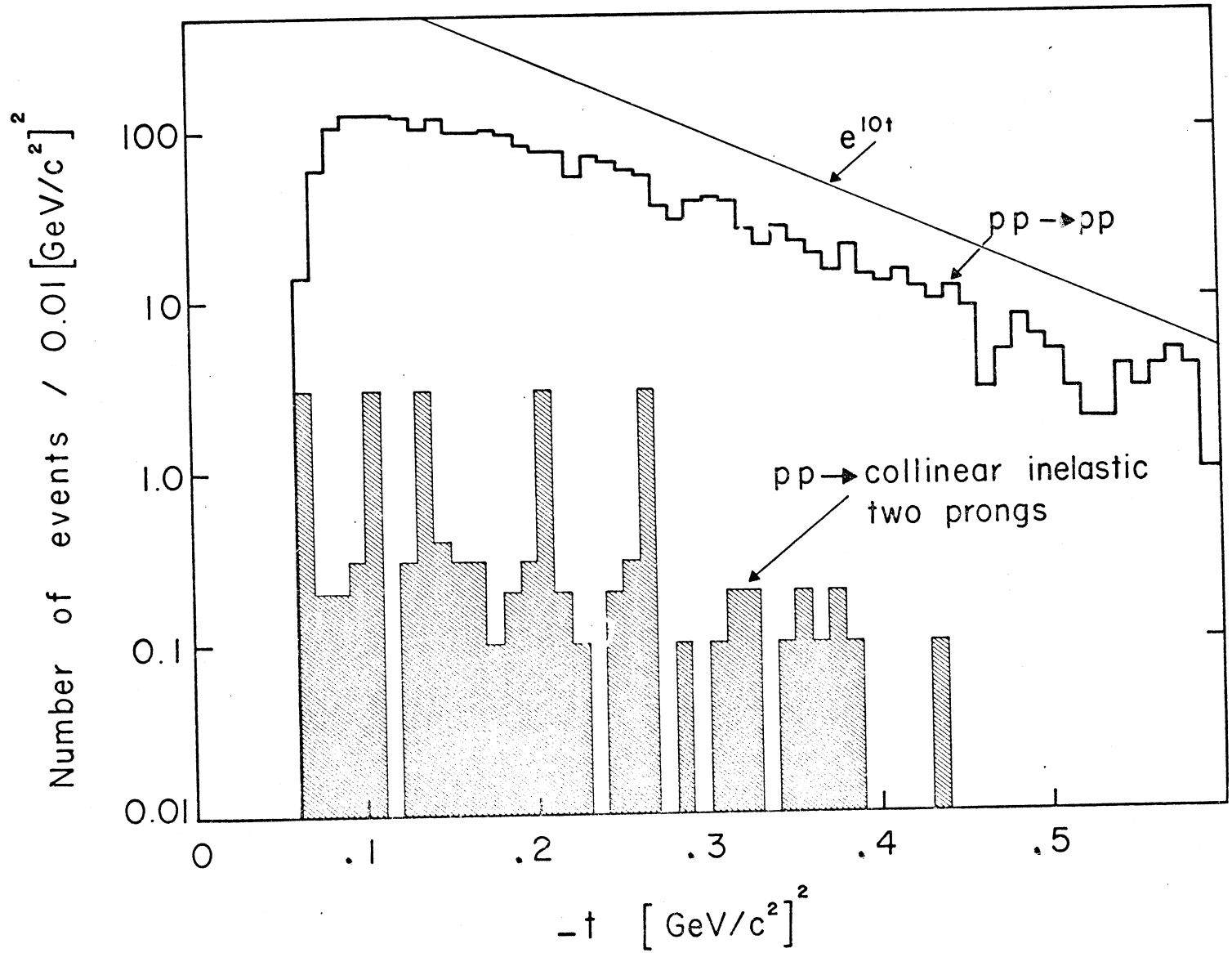
Number of events / 0.01 [GeV/c²]²
100
10
1.0
0.1
0.01
0
.1
.2
.3
.4
.5
-t [GeV/c²]²
e^10t
pp → pp
pp → collinear inelastic
two prongs

fig. 6

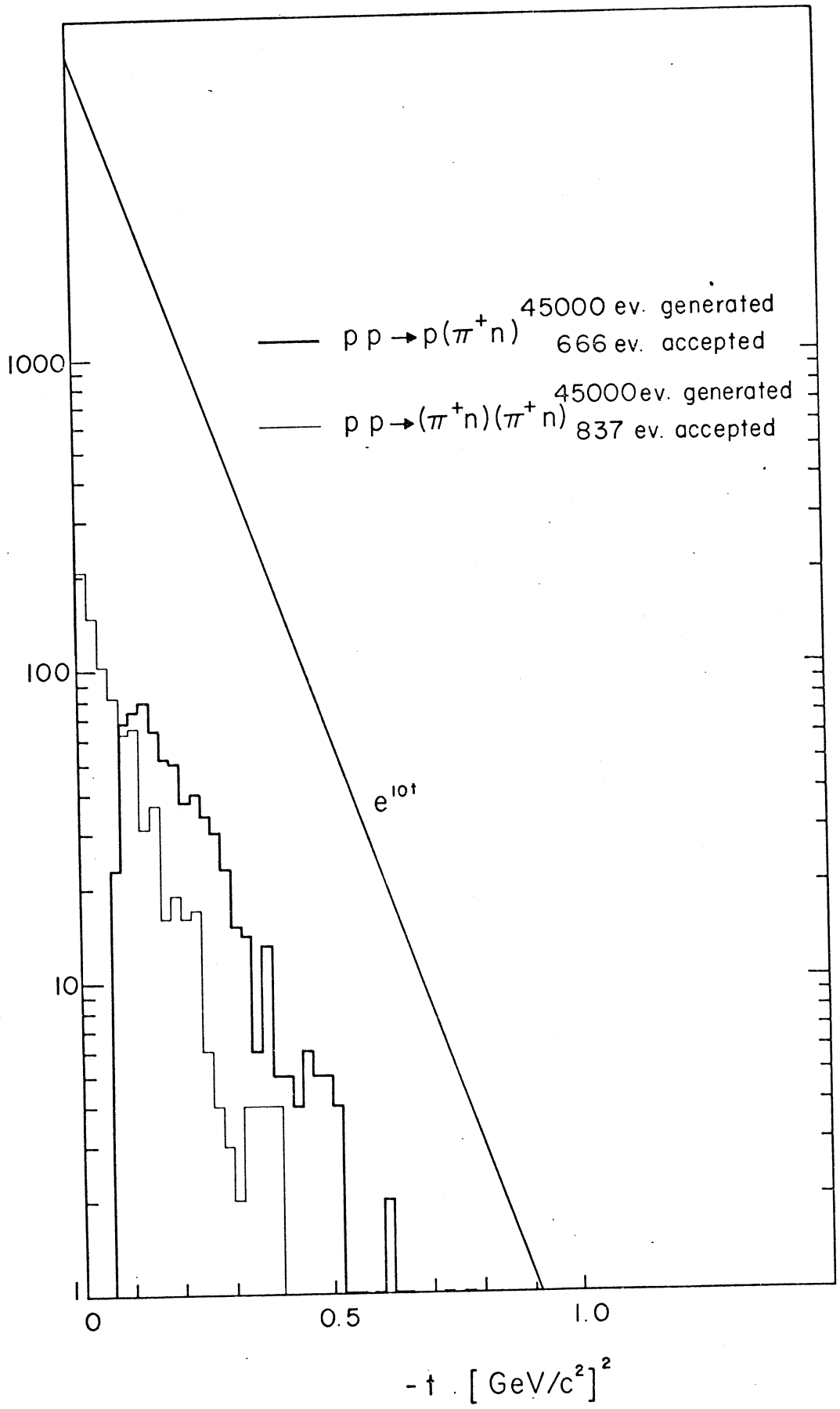
p p → p(π⁺n)
45000 ev. generated
666 ev. accepted
p p → (π⁺n)(π⁺n)
45000 ev. generated
837 ev. accepted
e^10t
1000
100
10
1
0
0.5
1.0
-t . [GeV/c²]²

fig. 7

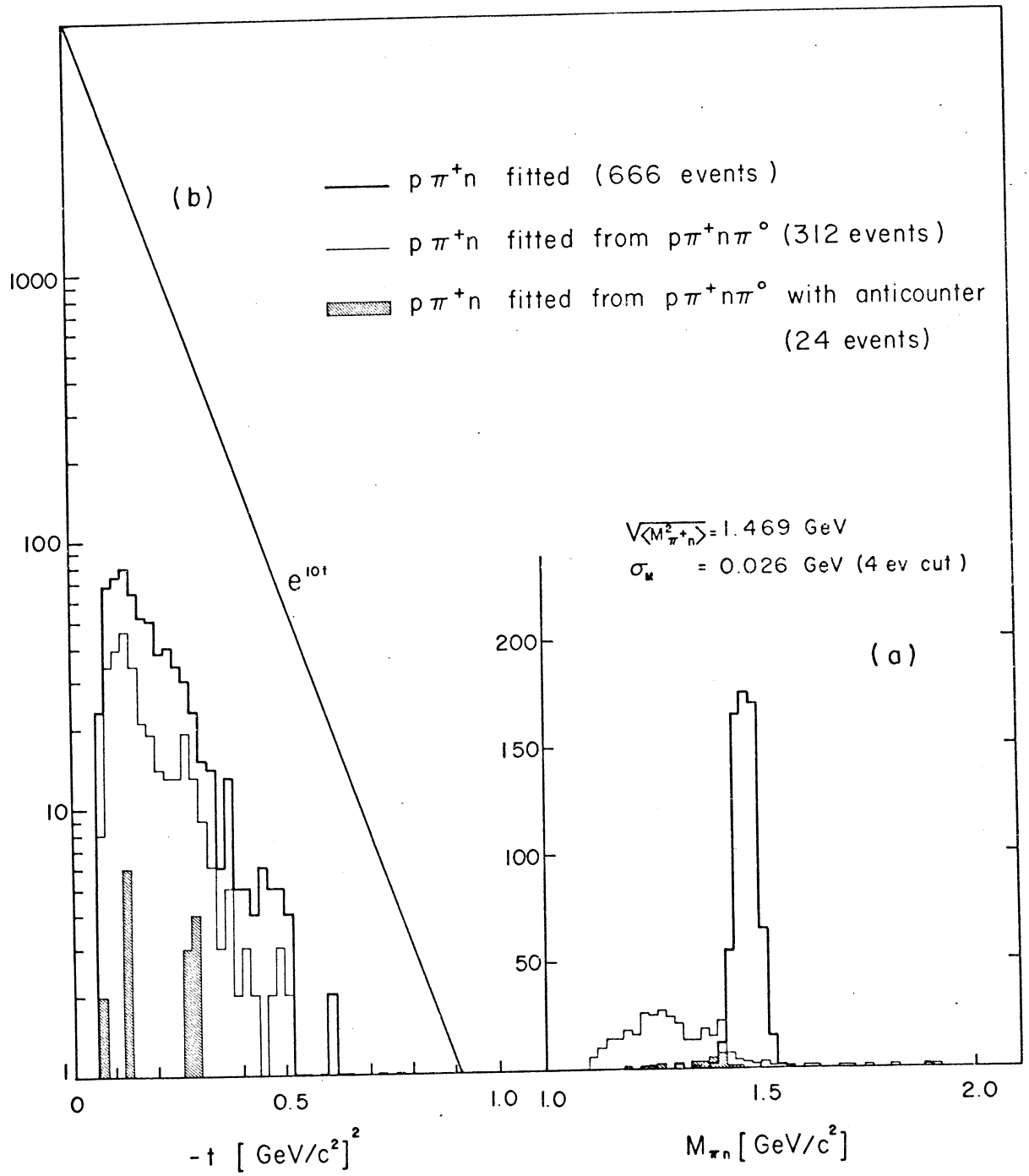
(b)
$p\pi^+n$ fitted (666 events)
$p\pi^+n$ fitted from $p\pi^+n\pi^\circ$ (312 events)
$p\pi^+n$ fitted from $p\pi^+n\pi^\circ$ with anticounter (24 events)
1000
100
10
1
e^{10t}
0
0.5
1.0
$-t\ [GeV/c^2]^2$
$\sqrt{\langle M^2_{\pi^+n}\rangle} = 1.469$ GeV
σ_M = 0.026 GeV (4 ev cut)
(a)
200
150
100
50
1.0
1.5
2.0
$M_{\pi n}\ [GeV/c^2]$

fig. 8

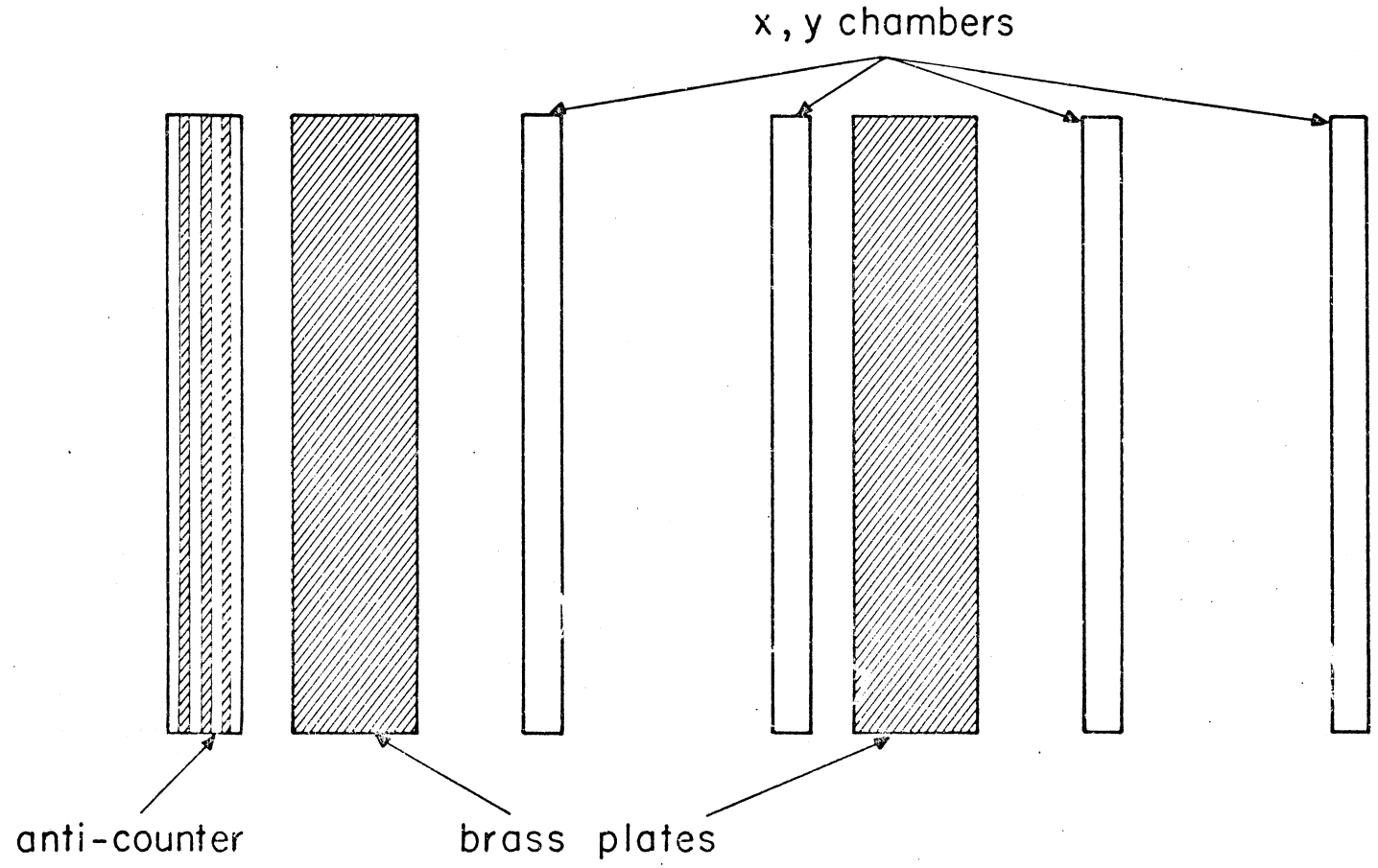

NEUTRON DETECTOR

fig. 9